From Slater to Mott-Heisenberg physics: The antiferromagnetic phase of the Hubbard model

Th. Pruschke and R. Zitzler

Center for electronic correlations and magnetism, Theoretical Physics III, Institute for Physics, University of Augsburg, 86135 Augsburg, Germany

We study the optical conductivity of the one-band Hubbard model in the Néel state at half filling at T=0 using the dynamical mean-field theory. For small values of the Coulomb parameter clear signatures of a Slater insulator expected from a weak-coupling theory are found, while the strongly correlated system can be well described in terms of a Mott-Heisenberg picture. However, in contrast to the paramagnet, we do not find any evidence for a transition between these two limiting cases but rather a smooth crossover as a function of the Coulomb interaction.

I. INTRODUCTION

The microscopic description of magnetism and metalinsulator transitions constitutes one of the major research activities in modern solid state theory. For example, transition metal compounds like V_2O_3 , LaTiO₃, NiS_{2-x}Se_x or the cuprates show metal-insulator transitions and magnetic order depending on composition, pressure or other control parameters.¹ One interesting and controversial question concerns the description of the optical properties of these materials, ^{2,3,4} in particular whether the fundamental physics is governed by the broken translational symmetry e.g. in the Néel state or rather by correlations, ^{5,6} i.e. the formation of so-called Hubbard bands with an energy gap of the order of the relevant Coulomb repulsion.

The simplest model showing both magnetism and a correlation induced metal-insulator transition (MIT) is the one-band Hubbard model 4

$$H = -\sum_{i,j,\sigma} t_{ij} c_{i\sigma}^{\dagger} c_{j\sigma} + \frac{U}{2} \sum_{i\sigma} n_{i\sigma} n_{i\bar{\sigma}} , \qquad (1)$$

where $c_{i\sigma}^{(\dagger)}$ annihilates (creates) an electron at site i with spin σ , $n_{i\sigma}=c_{i\sigma}^{\dagger}c_{i\sigma}$, t_{ij} denotes the hopping amplitude between sites i and j and U is the local Coulomb repulsion. Usually, one ignores longer range hopping processes and concentrates on nearest neighbor hopping only. Considerable progress in understanding the physics of this simple but nevertheless non-trivial model has been achieved in the last decade through the development of the dynamical mean-field theory (DMFT)^{7,8,9}. In particular, the phase diagram for the Hubbard model on a simple cubic lattice with nearest-neighbor hopping is very well understood^{8,9,10}. The major results are compiled in the schematic phase diagram in Fig. 1. At half filling the physics is dominated by an antiferromagnetic insulating phase (AFI) for all U > 0. For finite doping, the antiferromagnetic phase persists up to a critical doping $\delta_c^{10,11}$ and in addition shows phase separation^{11,12}. For very large values of U the antiferromagnetic phase is replaced by a small region of Nagaoka type ferromagnetism. ^{13,14}

An appealing property of the DMFT is the possibility to calculate transport quantities in a very simple fashion.

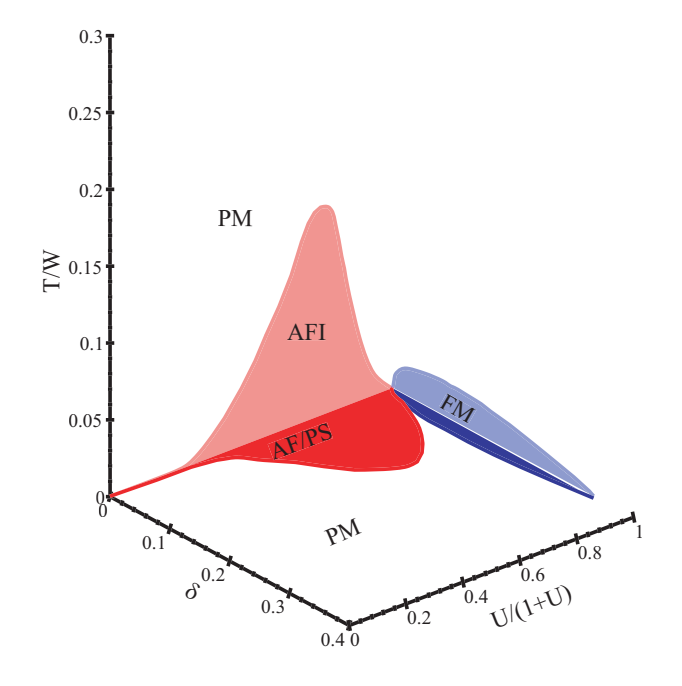


FIG. 1: Schematic DMFT phase diagram of the Hubbard model with nearest neighbor hopping on a simple cubic lattice. PM denotes the paramagnetic metal, AFI the antiferromagnetic insulator, FM the ferromagnetic metal and AF/PS phase separated antiferromagnetism.

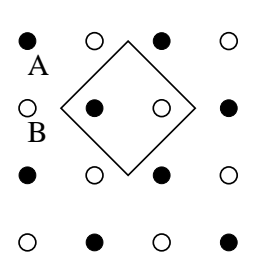
Due to the local nature of the theory, vertex corrections to the leading particle-hole bubble of the current-current correlation function vanish identically, 8,15 i.e. one needs to calculate the bare bubble only. This has been extensively used to study the optical conductivity and various other transport properties in the paramagnetic phase of the Hubbard model. 8,9,16 On the other hand, up to now a comparable investigation of the optical properties of symmetry broken phases, in particular the Néel state at half filling, has not been performed. However, such an investigation is interesting for several reasons. First, the insulating phase in real materials is in many cases accompanied by magnetic or orbital ordering, typically of the Néel type. To what extent the model (1) can describe the optical properties of ordered insulating phases has

up to now not been studied in detail. Second, it is well-known that the restriction of the Hubbard model to the paramagnetic state at half filling shows a metal-insulator transition 9,10,17,18 at a finite critical $U_c > 0$ which is of first order. 9,17 It might be argued that for the Néel state a similar situation can occur. At small U a weak coupling theory is expected to give accurate results, leading to a band or Slater insulator due to the doubled unit cell in the Néel state. At large U, on the other hand, the Hubbard model is known to reduce to an effective Heisenberg model model with localized moments from the onset. It is an open question whether these two limits are linked continously or via a phase transition at some finite value of the Coulomb interaction U.

The paper is organized as follows: In the next section the derivation of an expression for the optical conductivity in the Néel state is presented. The results obtained for the optical conductivity of the Hubbard model with nearest neighbor hopping on a simple cubic lattice at half filling are presented and discussed in section III. A conclusion and outlook finish the paper in section IV.

II. OPTICAL CONDUCTIVITY FOR THE NÉEL STATE IN DMFT

In the Néel state, the DMFT equations have to be modified to account for two inequivalent sublattices A and B (see Fig. 2, left panel) with self-energies $\Sigma^A \neq \Sigma^B.^{9,20}$ To this end, we introduce operators $a_{i\sigma}^{(\dagger)}$ and $b_{i\sigma}^{(\dagger)}$



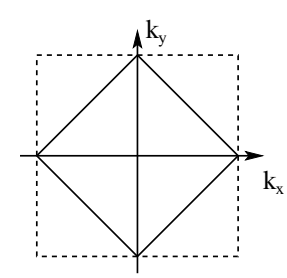


FIG. 2: Left: Schematic view of the AB sublattice decomposition suitable for the treatment of the Néel state. Right: Magnetic Brillouin zone (MBZ, 1. BZ of the Néel state).

which act on sublattice A and B respectively. In the case of nearest-neighbor hopping only, the kinetic part of the Hamiltonian (1) can then be written as

$$H_t = -t \sum_{\langle i,j \rangle} \sum_{\sigma} \left(a^{\dagger}_{i\sigma} b_{j\sigma} + b^{\dagger}_{j\sigma} a_{i\sigma} \right) .$$

After Fourier transforming this expression we obtain

$$H_t = \sum_{\mathbf{k}} \sum_{\mathbf{k}}' \Psi_{\mathbf{k}\sigma}^{\dagger} \begin{pmatrix} 0 & \epsilon_{\mathbf{k}} \\ \epsilon_{\mathbf{k}} & 0 \end{pmatrix} \Psi_{\mathbf{k}\sigma} ,$$

where we introduced the spinors

$$\Psi_{\mathbf{k}\sigma}^{\dagger} = \left(a_{\mathbf{k}\sigma}^{\dagger}\;,\; b_{\mathbf{k}\sigma}^{\dagger}\right) \;\;,\;\; \Psi_{\mathbf{k}\sigma} = \left(\begin{array}{c}a_{\mathbf{k}\sigma}\\b_{\mathbf{k}\sigma}\end{array}\right)$$

and $\epsilon_{\mathbf{k}}$ is the dispersion on the bipartite lattice. The prime on the sum indicates that the summation is over all values of \mathbf{k} in the *magnetic* Brillouin zone (MBZ) (see Fig. 2, right panel). Within this notation, the Green function becomes a matrix in the two sublattices,

$$G_{\mathbf{k}\sigma}(z) = \begin{pmatrix} \zeta_{\sigma}^{A} & -\epsilon_{\mathbf{k}} \\ -\epsilon_{\mathbf{k}} & \zeta_{\sigma}^{B} \end{pmatrix}^{-1} , \qquad (2)$$

where $\zeta_{\sigma}^{A/B}=z+\mu-\Sigma_{\sigma}^{A/B}$. From now on we employ the symmetry $\zeta_{\sigma}^{A}=\zeta_{\overline{\sigma}}^{B}\equiv\zeta_{\sigma}$ of the Néel state and drop the indices A/B. Using this formalism, the current operator is given by

$$\mathbf{j} = e \sum_{\sigma} \sum_{\mathbf{k}}' \Psi_{\mathbf{k}\sigma}^{\dagger} \begin{pmatrix} 0 & \mathbf{v}_{\mathbf{k}} \\ \mathbf{v}_{\mathbf{k}} & 0 \end{pmatrix} \Psi_{\mathbf{k}\sigma}$$

with $\mathbf{v_k} = \nabla_{\mathbf{k}} \epsilon_{\mathbf{k}}$ as usual. If we consider a lattice for which the conductivity tensor is diagonal, the elements $\sigma_{ii} \equiv \sigma$ can be calculated from (*D* is the spatial dimension of the lattice)

$$D \cdot \sigma(\omega) = \Re e \frac{1}{i\omega} \sum_{l=1}^{D} \langle \langle j_l; j_l \rangle \rangle_{\omega + i\delta}$$

with the current-current correlation function

$$\begin{split} &\langle\!\langle j_l; j_l \rangle\!\rangle_{i\nu} = e^2 \sum_{\sigma\sigma'} \sum_{\mathbf{k}\mathbf{k'}}^{\prime} v_{\mathbf{k}}^l v_{\mathbf{k'}}^l \\ &\times \langle\!\langle a_{\mathbf{k}\sigma}^{\dagger} b_{\mathbf{k}\sigma} + b_{\mathbf{k}\sigma}^{\dagger} a_{\mathbf{k}\sigma}; a_{\mathbf{k'}\sigma'}^{\dagger} b_{\mathbf{k'}\sigma'} + b_{\mathbf{k'}\sigma'}^{\dagger} a_{\mathbf{k'}\sigma'}^{} \rangle\!\rangle_{i\nu} \ . \end{split}$$

Again, due to the symmetry of the lattice, the index l can be dropped. The most important simplification arises from the locality of two-particle self-energies within the DMFT. 15,20,21 Note that in the present formulation the proper locality of the two-particle self-energies is still ensured, because in the DMFT as defined by equ. (2) no dynamical correlations between the A and B sublattices are introduced. In analogy to the paramagnetic case this allows us to carry out the $\mathbf k$ sums in diagrams containing two-particle self-energy insertions independently at each vertex. Since the single particle propagators only depend on $\mathbf k$ through the even function $\epsilon_{\mathbf k}$ and the $v_{\mathbf k}$ are of odd parity, the sum over their product vanishes. As a result, we obtain the exact expression for the current-current correlation function in the DMFT,

$$\langle\langle j; j \rangle\rangle_{i\nu} = -\frac{e^2}{\beta} \sum_{\omega_n} \sum_{\sigma} \sum_{\mathbf{k}}' v_{\mathbf{k}}^2$$

$$\times \left[\langle\langle a_{\mathbf{k}\sigma}; a_{\mathbf{k}\sigma}^{\dagger} \rangle\rangle_{i\omega_n + i\nu} \langle\langle b_{\mathbf{k}\sigma}; b_{\mathbf{k}\sigma}^{\dagger} \rangle\rangle_{i\omega_n} \right.$$

$$+ \left. \langle\langle b_{\mathbf{k}\sigma}; b_{\mathbf{k}\sigma}^{\dagger} \rangle\rangle_{i\omega_n + i\nu} \langle\langle a_{\mathbf{k}\sigma}; a_{\mathbf{k}\sigma}^{\dagger} \rangle\rangle_{i\omega_n} \right.$$

$$+ \left. \langle\langle b_{\mathbf{k}\sigma}; a_{\mathbf{k}\sigma}^{\dagger} \rangle\rangle_{i\omega_n + i\nu} \langle\langle b_{\mathbf{k}\sigma}; a_{\mathbf{k}\sigma}^{\dagger} \rangle\rangle_{i\omega_n} \right.$$

$$+ \left. \langle\langle a_{\mathbf{k}\sigma}; b_{\mathbf{k}\sigma}^{\dagger} \rangle\rangle_{i\omega_n + i\nu} \langle\langle a_{\mathbf{k}\sigma}; b_{\mathbf{k}\sigma}^{\dagger} \rangle\rangle_{i\omega_n} \right]$$

In terms of the Green function matrix elements in (2) we can rewrite this as

$$\langle\langle j;j\rangle\rangle_{i\nu} = -\frac{e^2}{\beta} \sum_{\omega_n} \sum_{\sigma} \sum_{\mathbf{k}}' v_{\mathbf{k}}^2$$

$$\times \left[G_{\mathbf{k}\sigma}^{AA} (i\omega_n + i\nu) G_{\mathbf{k}\sigma}^{BB} (i\omega_n) + G_{\mathbf{k}\sigma}^{BA} (i\omega_n + i\nu) G_{\mathbf{k}\sigma}^{AA} (i\omega_n) + G_{\mathbf{k}\sigma}^{BA} (i\omega_n + i\nu) G_{\mathbf{k}\sigma}^{BA} (i\omega_n) + G_{\mathbf{k}\sigma}^{AB} (i\omega_n + i\nu) G_{\mathbf{k}\sigma}^{AB} (i\omega_n) \right]$$

where

$$G_{\mathbf{k}\sigma}^{AA}(z) = \frac{\zeta_{\bar{\sigma}}}{\zeta_{\sigma}\zeta_{\bar{\sigma}} - \epsilon_{\mathbf{k}}^2} \ , \ G_{\mathbf{k}\sigma}^{BB}(z) = \frac{\zeta_{\sigma}}{\zeta_{\sigma}\zeta_{\bar{\sigma}} - \epsilon_{\mathbf{k}}^2}$$

and

$$G^{BA}_{{\bf k}\sigma}(z) = G^{AB}_{{\bf k}\sigma}(z) = \frac{\epsilon_{\bf k}}{\zeta_\sigma\zeta_{\bar\sigma} - \epsilon_{\bf k}^2} \ . \label{eq:GBA}$$

Next, we convert the k sum into an energy integral by introducing the average squared velocity,

$$\langle v^2 \rangle_{\epsilon} := \frac{1}{D \cdot N} \sum_{\mathbf{k}}' v_{\mathbf{k}}^2 \delta(\epsilon - \epsilon_{\mathbf{k}}) .$$
 (3)

Making furthermore use of the spectral representation of the Green functions, the frequency sum can be evaluated in a straightforward way and finally we obtain for the conductivity

$$\sigma(\omega) = c \sum_{\sigma} \int_{-\infty}^{0} d\epsilon \langle v^{2} \rangle_{\epsilon} \int_{-\infty}^{\infty} d\omega' \frac{f(\omega') - f(\omega' + \omega)}{\omega}$$

$$\times \left[A_{\sigma}(\epsilon, \omega') A_{\bar{\sigma}}(\epsilon, \omega' + \omega) + B_{\sigma}(\epsilon, \omega') B_{\sigma}(\epsilon, \omega' + \omega) \right] \tag{4}$$

with

$$A_{\sigma}(\epsilon,\omega) = -\frac{1}{\pi} \Im G_{\sigma}^{AA}(\epsilon,\omega + i\delta)$$

and

$$B_{\sigma}(\epsilon,\omega) = -\frac{1}{\pi} \Im G_{\sigma}^{AB}(\epsilon,\omega + i\delta) .$$

Here $f(\omega)$ is the Fermi function and c collects various constants. Note that the form (4) is reminiscent of the results found in the case of superconductivity, which is discussed at length e.g. in the book by Mahan.²² Consequently, one can expect to obtain similar features from the evaluation of (4).

In order to proceed with the calculation, it is necessary to specify the actual lattice structure and the corresponding non-interacting dispersion in equation (3). For the hypercubic lattice, $^{21} \langle v^2 \rangle_{\epsilon} \propto \rho^{(0)}(\epsilon)$ is a simple Gaussian, and the integration over ϵ can be performed analytically. For the details of this calculation see Appendix A.

III. RESULTS

In the following we present results for the optical properties of the Hubbard model on a simple hypercubic lattice with nearest neighbor hopping at half filling and T=0 in the DMFT. The hopping matrix element is chosen as $t = t^*/\sqrt{4D}$, which ensures the correct scaling of the kinetic energy in the limit $D \to \infty$. As energy unit it is convenient to use the bandwidth W of the system at U = 0. Since the Gaussian density of states (DOS) of the simple hypercubic lattice in the limit of infinite spatial dimensions has no real band edges, we take $W = 4t^*$ as a reasonable value. Note that for this choice of W, (i) the spectral weight of the Gaussian is exhausted by 99% between $\omega = \pm W/2$ and (ii) the paramagnetic metal-insulator transition will occur at $U_c \approx 4t^* = W^{10}$. The effective quantum impurity model of the DMFT is solved using Wilson's Numerical Renormalization Group method (NRG),²³ suitably extended for dynamical quantities and spin-polarization.^{24,25} The calculations were performed with a discretization parameter $\Lambda = 2$, keeping 800 states. Dynamical quantities were calculated with a Gaussian logarithmic broadening of 0.6. Occasional checks with 1600 states or smaller Λ showed sufficient robustness of the results.

A. Single-particle properties

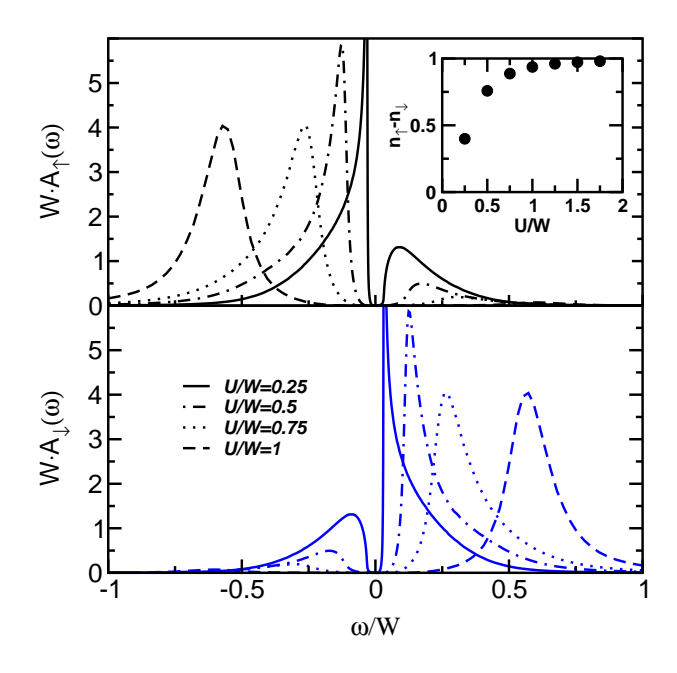


FIG. 3: Spin-resolved DOS for the antiferromagnetically ordered phase of the half-filled Hubbard model for different values of U/W. The inset shows the magnetization as function of U/W.

Before discussing the optical conductivity calculated

from (4), it is helpful to review the single particle properties. The spin resolved one-particle DOS calculated at T=0 for different values of U shows the expected insulating behavior with a clear gap at the Fermi energy for all U > 0. In particular for small values of $U \ll W$, the DOS shows nicely developed nesting singularities at the gap edges, which qualitatively follow the predictions of a weak coupling theory. 11 With increasing U these features get more and more smeared out, and for $U \gtrsim W$ the spectra resemble those of the Mott insulator.⁸ Note that the appearance of a gap in the DOS is of course accompanied by a vanishing imaginary part of the one-particle self-energy in this region. Neither the development of the DOS nor the magnetization as a function of U shown in the inset to Fig. 3 provide any evidence as to whether the limits $U \ll W$ and $U \gtrsim W$ will be linked smoothly or by some kind of transition.

B. Spin dynamics

Another interesting quantity is the dynamical magnetic susceptibility, whose low-energy behavior gives further insight into possible differences in spin and charge dynamics. In principle, it is also possible to calculate this quantity as a function of wave vector **q** within the DMFT. However, this requires the calculation of the local irreducible particle-hole self-energy, which is presently not possible within the NRG. Nevertheless,

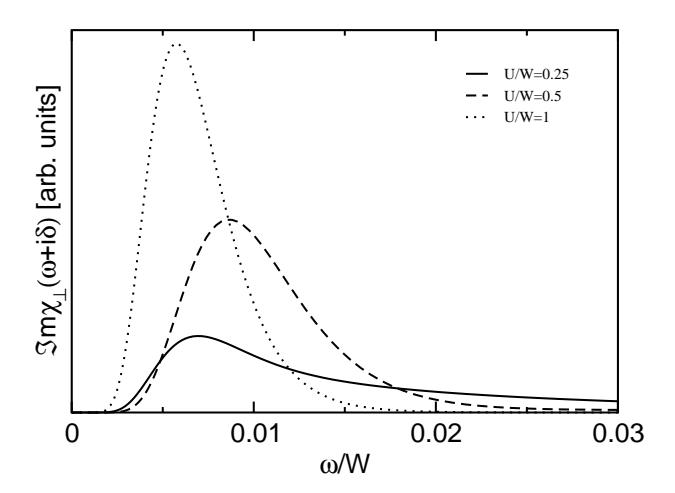


FIG. 4: Imaginary part of the local transverse magnetic susceptibility as a function of ω/W for U/W=0.25,~0.5 and 1, which shows a well-defined gap Δ_s as $\omega \to 0$. Only the part for $\omega > 0$ is shown. Note that Δ_s first increases with increasing U, but eventually decreases again.

for the current investigation, a reasonable approximation can be obtained from the local magnetic susceptibility,

$$\chi_{\perp}(z) = \frac{1}{N} \sum_{\mathbf{q}} \chi_{\perp}(\mathbf{q}, z) \ .$$

Since the ground state of our system is the Néel state, spin excitations require a minimum excitation energy, the spin gap Δ_s , which conventionally is read off $\Im m\chi_{\perp}(\mathbf{Q},\omega+i\delta)$ evaluated at the antiferromagnetic wave vector $\mathbf{Q} = (\pi, \pi, \ldots)$. However, the gaps at other \mathbf{q} vectors will be equal to or larger than Δ_s . Thus, even after summing over all q-values, the size of the gap in $\Im m\chi_{\perp}(\omega+i\delta)$ will be determined by Δ_s . The quantity $\Im m\chi_{\perp}(\omega+i\delta)$ on the other hand can easily be calculated from the NRG once the DMFT has converged. The results for three typical values of U/W are shown in Fig. 4, displaying a nice spin gap Δ_s as $\omega \to 0$. Evidently, the value of Δ_s first increases with increasing U but then decreases again, as is to be expected from the mapping of the Hubbard model to an antiferromagnetic Heisenberg model with $J \propto 1/U$ at large U. From the calculated $\Im m\chi_{\perp}(\omega+i\delta)$ one can directly extract the values for $\Delta_s(U)$. The results will be discussed below together with the charge gap obtained from the optical conductivity (see Fig. 7).

C. Optical conductivity and optical gap

The optical conductivity resulting from the spectra in Fig. 3 is shown in Fig. 5. Apparently, the overall behav-

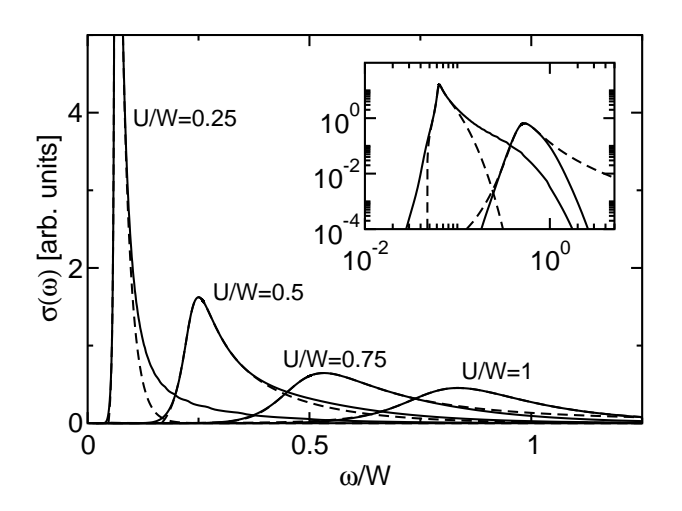


FIG. 5: Optical conductivity of the half-filled Hubbard model in the Néel phase for T=0 as a function of U. The full lines represent the calculated data, the dashed lines a fit with the function $\omega \cdot \sigma(\omega) = \Im m \left\{ e^{i\phi} \left(\omega - \omega_0 + i\gamma \right)^{-\alpha} \right\}$ (see text). The inset shows the curves for U/W=0.25 and U/W=0.75 using a logarithmic scaling.

ior seen in the DOS has its counter part in $\sigma(\omega)$. For small values of U, one finds a threshold behavior with a singularity, whereas for large U the optical conductivity closely resembles the one found in the paramagnetic insulator. Obviously, there are at least two interesting features in $\sigma(\omega)$. First, the behavior of $\sigma(\omega)$ in the vicinity of the maximum and second the actual value of the optical gap, i.e. the energy at which $\sigma(\omega) = 0$.

In order to address the first point we adopt the following line of reasoning. In the Hartree limit, i.e. without an

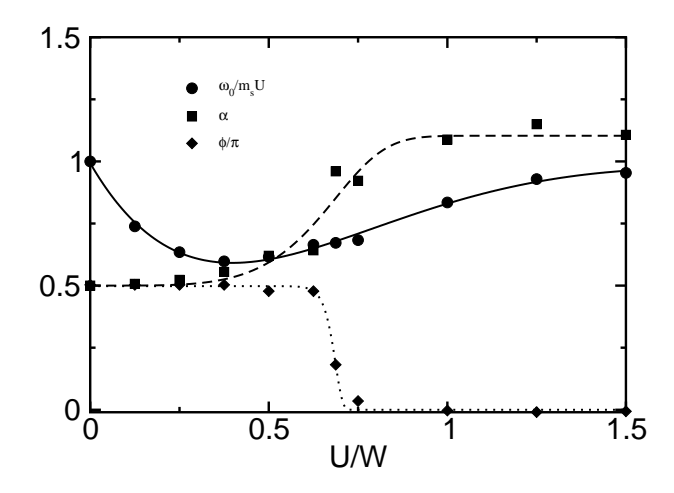


FIG. 6: Dependence of the fit parameters ω_0 , α and ϕ in (5) on U. The lines are meant as guides to the eye. Note the rather well defined change in (α, ϕ) from $(\alpha, \phi) = (1/2, \pi/2)$ to $(\alpha, \phi) = (1, 0)$ around U/W = 0.75.

imaginary part of the self-energy, an approximate evaluation of (4) yields

$$\omega \cdot \sigma(\omega) \propto \frac{\Theta(\omega - 2\Delta_0)}{\sqrt{\omega - 2\Delta_0}}$$

with $\Delta_0 = U m_s/2$ and $m_s = \langle n_{\uparrow} - n_{\downarrow} \rangle$. Since this behavior is governed by square root singularities in the integrand in (4) (see e.g. the explicit formula derived in the appendix), it is reasonable to assume that for a finite imaginary part of the self-energy the above singularity will become an algebraic function

$$\omega \cdot \sigma(\omega) \propto \Im m \left\{ \frac{e^{i\phi}}{(\omega - \omega_0 + i\gamma)^{\alpha}} \right\}$$
 (5)

with a general exponent α . The quantity γ approximately cares for the finite imaginary part introduced by the one-particle self-energy and ϕ allows for a more complex mixing of real and imaginary parts in the integral (4). The function (5) describes the behavior of $\sigma(\omega)$ in the vicinity of the maximum very nicely for all values of U (see dashed lines in Fig. 5); note that from the inset to Fig. 5 it is evident that for small U this algebraic form has the tendency to overestimate the optical gap, while at large U it is clearly underestimated.

Let us now turn to the behavior of the parameters ω_0 , α and ϕ shown in Fig. 6. As $U \to 0$, we expect that $\omega_0 = 2\Delta_0 = Um_s$, $\alpha = 1/2$ and $\phi = \pi/2$, i.e. $\omega \cdot \sigma(\omega) \propto \Re e (\omega - \omega_0 + i\delta)^{-1/2} = \Theta(\omega - \omega_0)/\sqrt{\omega - \omega_0}$. We indeed find the anticipated square-root singularity; however, even for small U/W, the value of ω_0 significantly deviates from the Hartree value, being systematically smaller but obviously approaching it as $U \to 0$.

For values U>W, the behavior of $\omega\cdot\sigma(\omega)$ is best described by a Lorentian, which becomes apparent from the values of α and ϕ obtained in this region, viz $\alpha\approx 1$ and $\phi=0$, meaning $\omega\cdot\sigma(\omega)\propto \Im m\left(\omega-\omega_0+i\gamma\right)^{-1}\propto 1/\left((\omega-\omega_0)^2+\gamma^2\right)$. In addition, the results for ω_0 together with $m_s\approx 1$ indicate that $\omega_0\approx U$, in agreement with the predictions of the Mott-Hubbard picture.

The behavior of the optical gap Δ_c , together with the

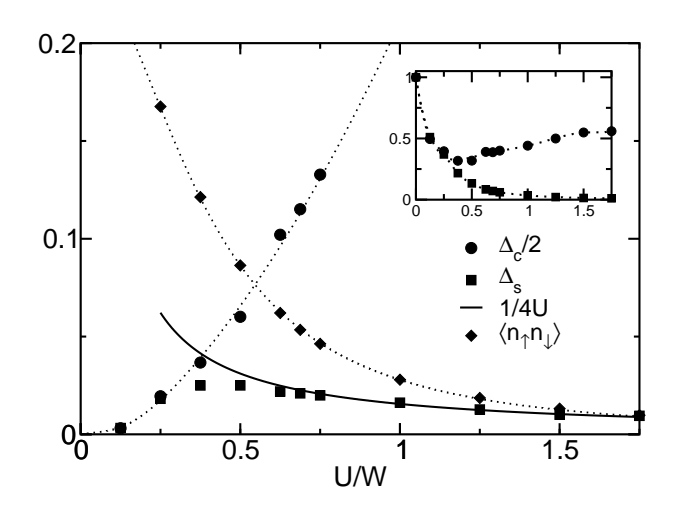


FIG. 7: Optical gap $\Delta_c/2$ (circles), spin gap Δ_s (squares) and double occupancy (diamonds) as function of U. The inset shows the gaps scaled with $Um_s/2$. Dotted lines are meant as guides to the eye. For small U both charge and spin gap are identical, while for large U we find $\Delta_c \propto U$ (see inset) and $\Delta_s \propto 1/U$ (full line in main panel).

spin gap Δ_s obtained from $\Im m \chi_{\perp}(\omega + i\delta)$ and the double occupancy $\langle n_{\uparrow} n_{\downarrow} \rangle$, is displayed in Fig. 7. The details of the method used to obtain Δ_c are discussed in appendix B.

For small U/W, the optical gap is exactly twice as large as the spin gap and, as becomes apparent from the inset, approaches the Hartree value m_sU as $U\to 0$. Again both quantities deviate systematically and by the same amount from the expected Hartree values even for the smallest U. Thus, even for U/W << 1 correlation effects are important and significantly modify the predictions from Hartree theory.^{12,26} For large U, on the other hand, we find $\Delta_c \propto U-W$, consistent with Mott-Hubbard localized states; furthermore, $\Delta_s \propto 1/U$ as expected from the mean-field theory of the Heisenberg model with a $J \propto 1/U$.

We find, however, no evidence that the Slater limit at $U/W \to 0$ and the Mott-Heisenberg limit at $U/W \to \infty$ are separated by some kind of phase transition. All results, including the variation of $\langle n_{\uparrow} n_{\downarrow} \rangle$ seen in Fig. 7, rather indicate that a smooth crossover takes place for $U/W \approx 3/4$.

IV. CONCLUSION AND OUTLOOK

While in the paramagnetic phase of the Hubbard model at half filling, when artificially extended to T=0, a true phase transition from a correlated metal to a Mott-Hubbard insulator at $U_c \approx W$ has been established, the situation in the physically more relevant Néel state has not been investigated in similar detail up to now. As a first step into this direction the properties in the ground state of the Hubbard model at half filling with particlehole symmetry have been discussed. We did confirm that the physical properties at small and large values of the Coulomb parameter U can be well described within a Slater and Mott-Heisenberg picture, respectively. In contrast to the paramagnetic Mott-Hubbard MIT we could not find any solid evidence for a similar transition in the Néel state; our data rather suggest a smooth crossover, which occurs at a value $U \lesssim W$. Even the double occupancy, which in the case of the paramagnetic MIT is an indicator of a phase transition, does not show any sign of an anomaly here.

A novel quantity we discussed was the spin gap, which we extracted from the local transverse spin susceptibility. The general behavior and size agree very well with exactly known limits. This shows that at least in cases where a well defined spin gap exists that becomes minimal at special points in the Brillouin zone, even the inspection of purely local dynamical susceptibilities can be sufficient.

There are, however, still several unanswered questions. First, the analytic form of the optical conductivity close to the optical gap and the precise value of this gap could not be obtained at present due to numerical problems when evaluating the integral (4). Especially for a more quantitative comparison with experiment this has to be improved in future work. Second, comparison with the data for V₂O₃ from ref. 5 show a nice agreement for the kinetic energy (obtained using the optical sum rule), but fail completely concerning the size of the optical gap. This is shown in Fig. 8, where we plot the kinetic energy scaled to its value for U = 0 (circles and left scale) and Δ_c/W (squares and right scale) vs. U/W. The open circle and square represent data for the kinetic energy and charge gap, respectively, extracted from ref. 5 for a V_2O_3 sample with $T_N \approx 50$ K. Obviously, with the present model, one largely overestimates the optical gap at intermediate values of U.

Of course the present investigation did concentrate on the simplest situation, viz a system with perfect particle-hole symmetry. In reality, electron hopping beyond nearest neighbors will destroy antiferromagnetism at small values of U and consequently lead to different gaps at intermediate values of U. On the other hand, the gaps at large U are controlled by Mott-Hubbard physics and will most likely change only little. A similar line of argument has in fact been invoked in ref. 5, too. A recent study of the properties of the magnetically frustrated Hubbard model indicates that this scenario is indeed very likely.²⁷

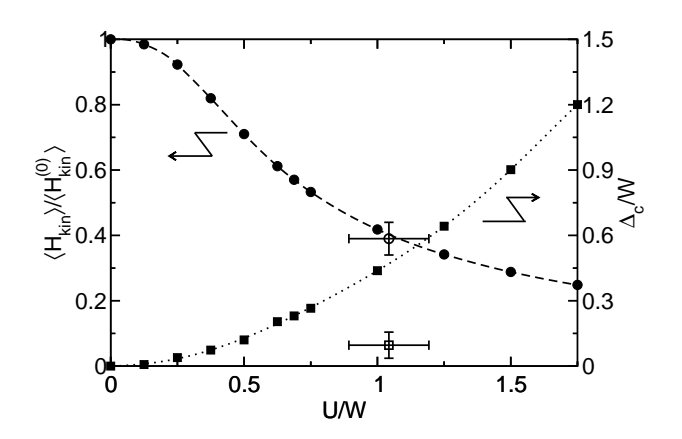


FIG. 8: Kinetic energy scaled to its value at U=0 (circles and left scale) and full optical gap Δ_c/W (squares and right scale) vs. U/W. The open circle and square with errorbars represent values for the scaled kinetic energy and Δ_c/W respectively, extracted from ref. 5 for the sample of V₂O₃ with $T_N \approx 50 \mathrm{K}$. Note that in ref. 5 D=W/2 and $\Delta=\Delta_c/2$.

Evidently, a further detailed investigation of the optical properties in the Néel state, in particular with more realistic band structures, is necessary and surely highly interesting. Work along this line is in progress.

Acknowledgments

We acknowledge useful conversations with D. Vollhardt, T.P. Deveraux, G. Uhrig, M. Potthoff, S. Kehrein and R. Bulla. This work was supported by the DFG through the collaborative research center SFB 484, the Leibniz Computer center and the Computer center of the Max-Planck-Gesellschaft in Garching.

APPENDIX A: FURTHER EVALUATION OF (4)

In this appendix we present details of the further evaluation of the energy integrals in equation (4) for the hypercubic lattice in the limit $D \to \infty$. In that case the density of states becomes a Gaussian, i.e. we need to calculate the two integrals

$$\int_{-\infty}^{\infty} d\epsilon \, e^{-\epsilon^2} A_{\sigma}(\epsilon, \omega') A_{\bar{\sigma}}(\epsilon, \omega' + \omega)$$

and

$$\int_{-\infty}^{\infty} d\epsilon \, e^{-\epsilon^2} B_{\sigma}(\epsilon, \omega') B_{\sigma}(\epsilon, \omega' + \omega) .$$

It is now convenient to split up the spectral functions into two parts, i.e.

$$A_{\sigma}(\epsilon,\omega) = A_{\sigma}^{-}(\epsilon,\omega) + A_{\sigma}^{+}(\epsilon,\omega)$$

with

$$A_{\sigma}^{\pm}(\epsilon,\omega) = -\frac{1}{2\pi} \Im m \frac{\zeta_{\bar{\sigma}}}{\sqrt{\zeta_{\sigma}\zeta_{\bar{\sigma}}}} \left(\frac{1}{\sqrt{\zeta_{\sigma}\zeta_{\bar{\sigma}}} \pm \epsilon} \right)$$

and ζ_{σ} as defined after equ. (2). In the same way we write

$$B_{\sigma}(\epsilon,\omega) = B_{\sigma}^{-}(\epsilon,\omega) - B_{\sigma}^{+}(\epsilon,\omega)$$

where now

$$B^{\pm}_{\sigma}(\epsilon,\omega) = -\frac{1}{2\pi} \Im m \frac{1}{\sqrt{\zeta_{\sigma}\zeta_{\bar{\sigma}}} \pm \epsilon} \ .$$

Using this notation and collecting equivalent terms, it can easily be verified that the following four integrals need to be evaluated:

$$I_1 = 2 \int_{-\infty}^{\infty} d\epsilon \, e^{-\epsilon^2} B_{\sigma}^{-}(\epsilon, \omega') B_{\sigma}^{-}(\epsilon, \omega' + \omega) ,$$

$$I_2 = -2 \int_{-\infty}^{\infty} d\epsilon \, e^{-\epsilon^2} B_{\sigma}^{-}(\epsilon, \omega') B_{\sigma}^{+}(\epsilon, \omega' + \omega) ,$$

$$I_3 = 2 \int_{-\infty}^{\infty} d\epsilon \, e^{-\epsilon^2} A_{\sigma}^{-}(\epsilon, \omega') A_{\bar{\sigma}}^{-}(\epsilon, \omega' + \omega)$$

and

$$I_4 = 2 \int_{-\infty}^{\infty} d\epsilon \, e^{-\epsilon^2} A_{\sigma}^{-}(\epsilon, \omega') A_{\bar{\sigma}}^{+}(\epsilon, \omega' + \omega) .$$

The further evaluation will be demonstrated for the first term. Using the notation

$$\alpha = \sqrt{\zeta_{\sigma}\zeta_{\bar{\sigma}}}\Big|_{\omega'+i\delta}$$
 and $\beta = \sqrt{\zeta_{\sigma}\zeta_{\bar{\sigma}}}\Big|_{\omega'+\omega+i\delta}$

we may write

$$\begin{split} B_{\sigma}^{-}(\epsilon,\omega')B_{\sigma}^{-}(\epsilon,\omega'+\omega) &= \\ &-\frac{1}{4\pi^{2}}\left[\left(\frac{1}{\overline{\alpha}-\epsilon}-\frac{1}{\alpha-\epsilon}\right)\left(\frac{1}{\overline{\beta}-\epsilon}-\frac{1}{\beta-\epsilon}\right)\right] \;\;, \end{split}$$

where the bar above a term denotes complex conjugation. The terms inside the brackets can be expanded further to yield

$$\begin{split} & \left[-\frac{1}{\overline{\alpha} - \overline{\beta}} \left(\frac{1}{\overline{\alpha} - \epsilon} - \frac{1}{\overline{\beta} - \epsilon} \right) + \frac{1}{\overline{\alpha} - \beta} \left(\frac{1}{\overline{\alpha} - \epsilon} - \frac{1}{\beta - \epsilon} \right) \right. \\ & \left. + \frac{1}{\alpha - \overline{\beta}} \left(\frac{1}{\alpha - \epsilon} - \frac{1}{\overline{\beta} - \epsilon} \right) - \frac{1}{\alpha - \beta} \left(\frac{1}{\alpha - \epsilon} - \frac{1}{\beta - \epsilon} \right) \right] \, . \end{split}$$

If we introduce the Faddeeva function

$$w(z) = \frac{i}{\pi} \int_{-\infty}^{\infty} dt \, \frac{e^{-t^2}}{z - t} = e^{-z^2} \operatorname{erfc}(-iz)$$

for complex arguments z with $\Im mz > 0$, we obtain

$$I_{1} = \frac{1}{2\pi i} \left[\frac{w(\alpha) - w(\beta)}{\alpha - \beta} - \frac{\overline{w(\alpha)} - \overline{w(\beta)}}{\overline{\alpha} - \overline{\beta}} - \frac{w(\alpha) + \overline{w(\beta)}}{\alpha - \overline{\beta}} + \frac{w(\alpha) + \overline{w(\beta)}}{\overline{\alpha} - \beta} \right]$$

where we have made use of the relation $w(-\overline{z}) = \overline{w(z)}$. The remaining three contributions can be obtained in a similar fashion. Finally, combining complex conjugate expressions, we arrive at the following result for the four integrals:

$$I_{1} = \frac{1}{\pi} \Im \left(\frac{w(\alpha) - w(\beta)}{\alpha - \beta} - \frac{w(\alpha) + \overline{w(\beta)}}{\alpha - \overline{\beta}} \right)$$
(A1)

$$I_{2} = -\frac{1}{\pi} \Im \left(\frac{w(\alpha) - \overline{w(\beta)}}{\alpha + \overline{\beta}} - \frac{w(\alpha) + w(\beta)}{\alpha + \beta} \right)$$
 (A2)

$$I_{3} = \frac{1}{\pi} \Im \left(\gamma \delta \frac{w(\alpha) - w(\beta)}{\alpha - \beta} - \gamma \overline{\delta} \frac{w(\alpha) + \overline{w(\beta)}}{\alpha - \overline{\beta}} \right)$$
(A3)

$$I_{4} = \frac{1}{\pi} \Im \left(\gamma \overline{\delta} \frac{w(\alpha) - \overline{w(\beta)}}{\alpha + \overline{\beta}} - \gamma \delta \frac{w(\alpha) + w(\beta)}{\alpha + \beta} \right)$$
(A4)

where we have introduced

$$\gamma = \frac{\zeta_{\bar{\sigma}}}{\sqrt{\zeta_{\sigma}\zeta_{\bar{\sigma}}}} \bigg|_{\omega' + i\delta} \quad \text{and} \quad \delta = \frac{\zeta_{\sigma}}{\sqrt{\zeta_{\sigma}\zeta_{\bar{\sigma}}}} \bigg|_{\omega' + \omega + i\delta}$$

A further analytical evaluation of the remaining integration over ω' in equation (4) using eqs. (A1) – (A4) is possible only for $\zeta_{\sigma} \to \omega - \sigma \Delta_0 + i\delta$. In this case, the square-roots appearing in the functions α and β lead to a typical threshold behavior of the form²²

$$\omega \cdot \sigma(\omega) \propto \frac{\Theta(\omega - 2\Delta_0)}{\sqrt{\omega - 2\Delta_0}}$$
.

The appearence of this threshold singularity also shows that a further numerical evaluation of the remaining integral over ω' in equation (4) will become problematic in regions where the imaginary part of the one-particle self-energy becomes small, because the integrand will develop a strongly singular behavior. In particular, this makes a precise numerical evaluation of the optical conductivity near the threshold impossible.

APPENDIX B: THE OPTICAL GAP

While the definition of the optical gap is straight forward, the extraction of numbers from the numerical data

appears to be rather problematic for two simple reasons. First, the spectra calculated with NRG have an unavoidable intrinsic broadening, which becomes especially severe for the Hubbard bands at larger values of U/W. Second, as $\omega \ll \omega_0$, the imaginary part of the one-particle self-energy becomes negligible, and the singular structure of the integrand (A1) – (A4) entering into (4) makes additional broadening necessary to allow for a stable numerical integration. Together both effects very efficiently mask the true ω -dependence close to the optical gap, in particular for larger U/W.

In order to nevertheless have an unambiguous working procedure that allows to extract a reasonable approximation to the true optical gap from our numerical data, we postulate that $\omega \cdot \sigma(\omega) \propto \Theta(\omega - 2\Delta_0) \cdot (\omega - 2\Delta_0)^{\alpha}$ for ω in the region where (5) starts to deviate substantially from the data and choose a minimal α such that it produces a reasonable fit for all values of U (see Fig. 9 for selected results). We find $\alpha = 5/2^{28}$ and an optical gap Δ_c which is consistent with the spin gap Δ_s as $U \to 0$. The good agreement of these two differently calculated quantities (see inset to Fig. 7) also serves as an a posteriori check for the procedure used to determine Δ_c . In view of a possible comparison to experimental results⁵ this situation is, of course, not satisfying. For this purpose a more thorough and possibly analytical evaluation

of $\sigma(\omega)$ close to Δ_c would be desirable. Unfortunately, the complicated form of the integrals in (4) so far have allowed for an analytical evaluation only in the Hartree limit.

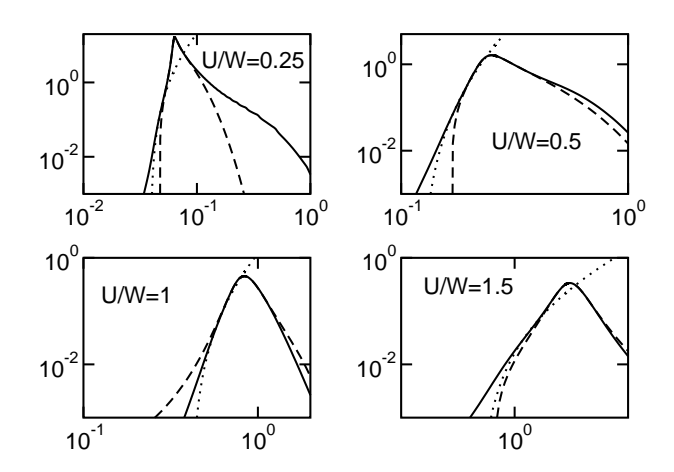


FIG. 9: Results for the fits to $\sigma(\omega)$ (full lines) with function (5) for $\omega \approx \omega_0$ (dashed lines) and $\Theta(\omega - 2\Delta_0) \cdot (\omega - 2\Delta_0)^{5/2}$ in the low- ω region (dotted lines) for several values of U/W.

¹ M. Imada, A. Fujimori, and Y. Tokura, Rev. Mod. Phys. 70, 1039 (1998).

² J.C. Slater, Phys. Rev. **82**, 538 (1951).

³ N.F. Mott, Philos. Mag. **6**, 287 (1961).

J. Hubbard, Proc. R. Soc. London A276, 238 (1963);
 M.C. Gutzwiller, Phys. Rev. Lett. 10, 59 (1963);
 J. Kanamori, Prog. Theor. Phys. 30, 275 (1963).

⁵ G.A. Thomas, D.H. Rapkine, S.A. Carter, A.J. Millis, T.F. Rosenbaum, P. Metcalf and J.M. Honig, Phys. Rev. Lett. **73**, 1529 (1994).

⁶, A. Loidl, private communication.

W. Metzner und D. Vollhardt, Phys. Rev. Lett. **62**, 324 (1989).

⁸ T. Pruschke, M. Jarrell and J.K. Freericks, Adv. Phys. **42**, 187 (1995);

⁹ A. Georges, G. Kotliar, W. Krauth and M.J. Rozenberg, Rev. Mod. Phys. 68, 13 (1996).

¹⁰ M. Jarrell and Th. Pruschke, Z. Phys. B**90**, 187 (1993).

¹¹ R. Zitzler, Th. Pruschke, R. Bulla, Eur. Phys. J. B 27, 473 (2002).

P.G.J. van Dongen, Phys. Rev. Lett. 67, 757 (1991); Phys. Rev. B50, 14016 (1994).

¹³ Y. Nagaoka, Phys. Rev. **147**, 392 (1966).

¹⁴ Th. Obermeier, Th. Pruschke and J. Keller, Phys. Rev. B56, R8479 (1997).

¹⁵ A. Khurana, Phys. Rev. Lett. **64**, 1990 (1990).

¹⁶ J.K. Freericks, T.P. Deveraux, and R. Bulla, Phys.

Rev. B**64**, 233114 (2001); J.K. Freericks, T.P. Deveraux, R. Bulla and Th. Pruschke, Phys. Rev. B **67**, 155102 (2003).

¹⁷ R. Bulla, Phys. Rev. Lett. **83**, 136 (1999).

¹⁸ R. Bulla, T.A. Costi, D. Vollhardt Phys. Rev. B**64**, 045103 (2001).

¹⁹ P. Fulde, Electron correlations in molecules and solids, Springer, Berlin (1995).

²⁰ U. Brandt und C. Mielsch, Z. Phys. B**82**, 37 (1991).

²¹ Th. Pruschke, D.L. Cox, M. Jarrell, Phys. Rev. B47, 3553 (1993).

²² G. Mahan, Many-Particle Physics, Plenum Press, New York (1990).

K.G. Wilson, Rev. Mod. Phys. 47, 773 (1975); H.R. Krishna-murthy, J.W. Wilkins, and K.G. Wilson, Phys. Rev. B 21, 1003 (1980); *ibid.* 21, 1044 (1980).

 $^{^{24}\,}$ R. Bulla, A.C. Hewson and Th. Pruschke, J. Phys. – Condens. Matter ${\bf 10},\,8365$ (1998).

²⁵ T.A. Costi, Phys. Rev. Lett. **85**, 1504(2000); W. Hofstetter, Phys. Rev. Lett. **85**, 1508 (2000).

²⁶ S. Moukouri and M. Jarrell, Phys. Rev. Lett. **87**, 167010 (2001).

²⁷ R. Zitzler, N. Tong, Th. Pruschke, and R. Bulla, cond-mat/0308202.

 $^{^{28}}$ The value $\alpha=3/2$ used in ref. 5 does not lead to a satisfying description.